Brain-Dedicated Emission Tomography Systems: A Perspective on Requirements for Clinical Research and Clinical Needs in Brain Imaging

RESEARCH applications of human brain positron emission tomography (PET) imaging have been in place for over 40 years. The unique combination of quantitative PET instrumentation and reconstruction, novel radiotracers, and kinetic modeling has led to the development and application of a huge number of imaging paradigms. These have been applied to the understanding of normal function and pathophysiology, the development of drugs for neuropsychiatric disorders, and the study of drug interactions with the brain. I have had been fortunate to be part of this great endeavor throughout my research career, using brain-dedicated PET scanners, such as the HRRT [item 1) in the Appendix]. Over time, these systems have offered important advantages over whole-body systems. However, due to the limited clinical market for brain PET imaging, scanner manufacturers have focused exclusively on large field-of-view systems for the past two decades [item 2) in the Appendix]. The goal of this perspective is to share a viewpoint on the utility of brain-dedicated PET systems for human research, particularly in the context of novel radiotracers with dynamic studies using kinetic modeling.

What can a brain-dedicated PET system provide to the research community that current state-of-the-art whole body systems cannot? Like most things in PET and nuclear medicine, the answer involves the usual suspects: sensitivity and resolution.

High Sensitivity: Sensitivity is always an important factor for PET. It allows a lower injected dose with comparable data quality or provides a useful count level at later times postinjection. When combined with high resolution, it produces sufficient counts for the smaller voxels, yielding more precise quantification. In our experience with the HRRT, the system's high sensitivity has been particularly important for C-11 tracers. Many successful C-11 tracers can reach an apparent equilibrium (transient equilibrium [item 3) in the Appendix]) within 1 h, allowing a useful measurement of quantitative binding parameters, such as volume of distribution (V_T) and binding potential (BP_{ND}) [item 4) in the Appendix]. However, if the tracer's kinetic rates are slower, with a conventional whole-body system there will be too few counts available in the period beyond 60 min postinjection. With a high sensitivity machine like the HRRT, we routinely collect dynamic C-11 data to 120 or even 150 min. This has allowed us to make reliable quantitative measurements of norepinephrine transporters with ^{11}C-MRB [item 6) in the Appendix], serotonin transporters with ^{11}C-AFM [item 6) in the Appendix], dopamine transporters with ^{11}C-PHNO [item 7) in the Appendix], and kappa opioid receptors with ^{11}C-GR103545 [item 8) in the Appendix]. Interestingly, it is the brain regions with the highest binding (highest target concentration) that require the most time to approach equilibrium. This has permitted these radiotracers to provide information about most or all brain regions, not just the regions with lower target densities which have faster kinetics.

High sensitivity is also of critical importance to produce parametric images, where each voxel is fitted to a kinetic model, and the estimated parameters are displayed as an image. In many cases, some image smoothing is necessary to remove noise and outliers in these parametric images. The modeling and image processing communities have spent much effort to find ways to reduce noise in these images, whether it be through approaches such as principal component analysis (PCA) [item 9) in the Appendix], use of wavelet transforms [item 10) in the Appendix], combined spatial/temporal smoothing [item 11) in the Appendix], or direct reconstruction of parametric images [item 12), 13) in the Appendix]. While all these approaches have important utility, in each case, the method must be carefully tuned to the tracer and the application. For example, when PCA is applied to a dynamic image set, and there is a small region with very different kinetics, if two few components are included in the analysis, that region could be removed from the data. Thus, in general, it is always better if the counts are available in the first place. For example, for our synaptic density imaging agent which binds to SV2A in presynaptic vesicles [item 14) in the Appendix], thanks to both high brain uptake and the high sensitivity of the HRRT, parametric images can be created without smoothing, i.e., at full image resolution [item 15) in the Appendix].

High Resolution: One potential advantage of a brain-dedicated system would be ultrahigh resolution. Our field has ample experience producing very high resolution small animal systems, so the technical challenges are well known. The ability to image small structures is very important in clinical research. There are several examples of brain neurotransmitter systems where small nuclei, often located in the midbrain, are the source of the neurons which produce the neurotransmitter. This includes the locus coeruleus for norepinephrine, the raphe nuclei for serotonin, and the substantia nigra for dopamine. These regions have been implicated in many diseases, with the best example being the nigra and Parkinson's disease (PD). Thus, the ability to simultaneously image these subcortical "source" regions, and their upstream projection areas (the striatum for dopamine), is of huge utility since often

Digital Object Identifier 10.1109/TRPMS.2019.2912129

these regions have complex and complementary changes in disease [item 16) in the Appendix].

Having systems with ultrahigh resolution will also allow us to look at regions of focal defects, e.g., in neurodegenerative disease. In the last decade or so, imaging of the deposition of β-amyloid with ^{11}C-PIB and other radiotracers [item 17) in the Appendix] has become common place. Ironically, amyloid deposition as measured by these radiotracers in early and advanced dementias is quite widespread and not focal; thus, imaging of β-amyloid can easily be accomplished with conventional-resolution systems. For other markers, the regional increases (e.g., for tau imaging [item 18) in the Appendix]), or decreases (e.g., for FDG [item 19) in the Appendix] and synaptic density [item 20) in the Appendix]) are more focal. In patients with well-established disease, the magnitude of regional changes is large. However, higher resolution will become more important as we image younger subjects, i.e., potential future dementia patients scanned long before cognitive deficits emerge. Here, the ability to detect small changes in small regions will be of huge benefit to select patients for the (hopefully) soon-to-emerge treatments for dementia. For example, in synaptic density imaging [item 20) in the Appendix], the changes appear in the hippocampus and the nearby entorhinal cortex; careful separation of these regions will be important to both understand the natural progression of dementia, but also to accurately identify patients at an early enough stage where treatment can have its biggest long-term effect.

There are, of course, technical reasons why higher resolution would be of great use. One obvious advantage is to minimize the partial volume effect. While there have been many advances in partial volume correction [item 21) in the Appendix], all of these methods depend heavily on their respective assumptions, including accurate registration with anatomical MR images. The magnitude of the partial volume effect varies tremendously based on the image resolution and the local contrast, which is often time-dependent. Truly accurate partial volume correction is nearly impossible in very small regions (like those in the midbrain listed above), where there is no easy way to accurately define the size and borders of the structure. Thus, in the same way that higher counts obviate the need for fancy noise-reduction methods, higher resolution minimizes the need for partial volume correction. It also means that we can accurately differentiate anatomical tissue atrophy from loss of PET imaging targets in the remaining brain tissue.

For kinetic modeling, measurement of the input function is needed for quantification, and high-resolution images open the possibility of image-derived input functions (IDIF). Many IDIF methods have been proposed for brain studies. Since the carotid arteries have an average diameter of ~4–6 mm, this is clearly challenging for conventional-resolution PET scanners and most of the current successful IDIF methods require some blood sampling for scaling, even for FDG. Both simulation and clinical data suggest that a reliable, and completely blood-sample free, procedure is not currently available [item 22) in the Appendix]. This is even the case for the HRRT [item 23) in the Appendix]. Thus, even higher resolution scanners will be very helpful to eventually achieve accurate IDIFs. For input functions, there are two caveats, however: 1) for many radiotracers, correction for radiolabeled metabolites will be needed and 2) for precise measurements in small blood vessels, high sensitivity will be needed (or noise reduction methods) to minimize variance.

In addition to high sensitivity and high resolution, a critically important characteristic of a next-generation brain-dedicated system should be continuous head motion tracking and correction, in order to achieve the best possible image resolution. Using a tool mounted on a cap on each subject's head and the Polaris Vicra system, we have performed event-by-event head motion correction in over 3000 dynamic PET brain research studies on the HRRT [item 24), 25) in the Appendix]. However, the current system is not foolproof, in that, in a small percentage of cases, there is slippage of the cap, and the motion data are corrupted. Also, in a large percentage of cases, this kind of continuous head motion correction is not necessary, i.e., software-based registration works well, so long as the proper registration between emission and attenuation images is performed. However, one challenge in software-based correction is in low-count frames, particularly at late times in ^{11}C-studies. An alternative approach is to detect motion based on PET raw data, i.e., a data-driven approach [item 26) in the Appendix]. In many cases, the PET raw data provides excellent sensitivity to detect motion, but more work is needed to be able to use this to directly correct motion. Further, data-driven methods must be validated for each radiotracer, since the emission distribution will affect accuracy. Perhaps, the best approach is tracking the head position with cameras using markerless approaches, i.e., using head and face features to derive the transformation matrices [item 27) in the Appendix]. Ideally, this technology should be integrated into the brain-dedicated PET scanner of the future.

In summary, for brain PET applications to continue to expand both in research and for eventual clinical applications, there is an important need for higher-resolution, higher-sensitivity PET systems. This next step can be most readily achieved with brain-dedicated systems. The smaller bore will increase the sensitivity and the smaller total detector volume will make it less cost-prohibitive to use smaller, higher-resolution detection elements. When this geometry is combined with the latest improvements in time-of-flight technology (TOF resolution of 200 ps or better, [item 28) in the Appendix]), the net improvement in sensitivity over the HRRT will be substantial. Such systems are likely to have their biggest impact in two areas: 1) imaging of neurodegenerative disorders, especially to detect the first earliest stages of disease and 2) for neuroimaging of children and adolescents, where the high sensitivity will allow ultralow dose imaging. With these ever-improving imaging technologies combined with the ongoing development of novel radiotracers, like those for synaptic imaging, the future for brain PET remains very bright.

Clinical Needs in Brain Imaging: Physician-Scientist's Point of View

The clinical needs for imaging of the brain are both vast in their importance as well as their diversity. Two large disease domains on the cusp of major developments are neuro-oncology and neurodegenerative disorders. The burgeoning field of theranostics crosses disease boundaries. Advanced

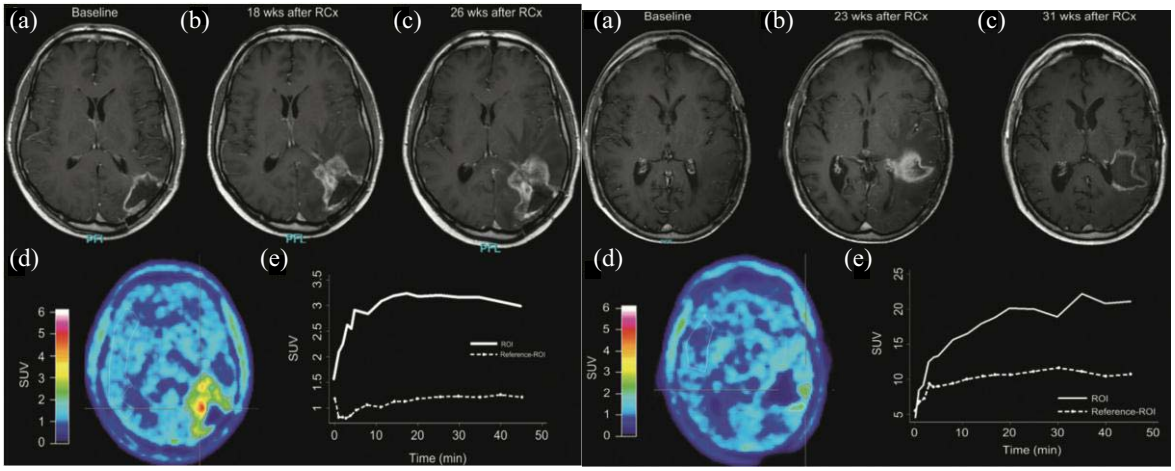

Fig. 1. O-(2-[18F]fluoroethyl)-L-tyrosine PET imaging has the potential to improve the differentiation of pseudo-progression from true progression of brain tumors. The panel on the left displays an area of increased enhancement on MRI (top row) that also shows increased uptake of radiotracer on PET (bottom row) consistent with true progression. The panel on the right displays an area of increased enhancement on MRI (top row) that shows uptake of radiotracer on PET similar to background (bottom row) consistent with pseudo-progression.

imaging can also make exciting discoveries in basic biology. As a physician-scientist, I contribute both to moving the field of medicine into the future and also taking care of patients. "In the real world," physicians place patient safety as a top priority and also navigate complex socioeconomic issues. Through lessons from the past and present, this paper provides a glimpse into the near future of the clinical needs in imaging of the brain.

A. Neuro-Oncology

1) Tumor Recurrence Versus Pseudo-Progression: The combination of MRI and PET has demonstrated improvement in the diagnosis of gliomas [item 29) of the Appendix]. A common dilemma with treated brain tumors is distinguishing true recurrence of tumor from inflammation or pseudo-progression.

FDG is extensively utilized in oncologic imaging but can have false positives due to inflammation and can be problematic specifically in the brain due to the high background cortical uptake. Therefore, other PET tracers have been investigated for distinguishing recurrence from pseudo-progression in the brain. For example, FET-PET utilizes a tyrosine (amino acid) analog which has lower background brain activity than FDG and potentially greater specificity for tumor versus inflammation [item 30) of the Appendix]. The example in Fig. 1 illustrates its use in distinguishing disease progression from pseudo-progression. Another amino acid analog used as a PET radiotracer is fluciclovine. Karlberg *et al.* [item 31) of the Appendix] exhibited a potential use of PET earlier in the management of brain tumors. The authors found that increasing uptake of fluciclovine correlated with higher grade components of the tumor, thus PET may help direct biopsy and thus avoid underestimating the grade of the tumor. Fluciclovine is particularly interesting as a potential radiopharmaceutical for brain imaging since it was approved by the United States Food and Drug Administration (USFDA) in 2016 for suspected recurrence of prostate cancer.

2) Theranostics: An area of considerable promise in neuro-oncology is theranostics. A proposed definition is "A theranostic system integrates some form of diagnostic testing to determine the presence of a molecular target for which a specific drug is intended" [item 32) of the Appendix]. I would suggest the following modified definition for a more imaging-oriented focus: "Noninvasive imaging technique and/or analysis to improve patient selection for the presence of target molecule or target profile for a specific therapy."

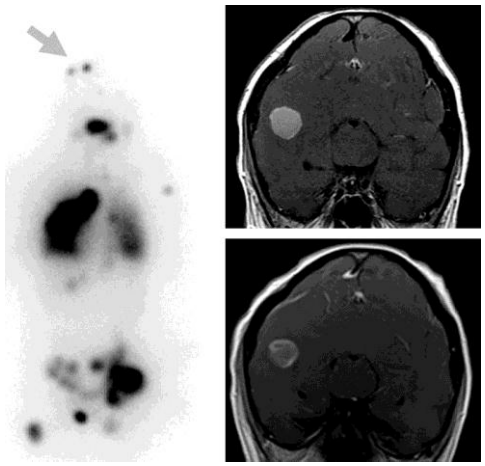

Fig. 2. Anterior planar imaging (left image) from head to upper thigh after administration of radioiodine demonstrates widespread metastatic disease in the brain, lungs, and skeleton. Arrow indicates brain metastases. MRI post GBCA in the coronal plane prior to therapy (top right) demonstrates a homogeneously enhancing metastasis (orange circle). MRI post GBCA in the coronal plane after therapy with iodine-131 (bottom right) demonstrates decreased enhancement of the metastasis (orange circle) consistent with partial response.

Theranostics has its foundation in nuclear medicine. The paradigm of using radioactive iodine-131 for diagnosis and treatment of thyroid disease is elegantly logical and effective. Thyroid tissue is the only tissue in the body that specifically accumulates iodine, and therefore, the beta-emitting radionuclide iodine-131 benefits from this natural targeting for a wide therapeutic window. For hyperthyroidism, radioactive iodine is used for both imaging and measuring uptake in the thyroid gland in order to determine a proper dose of radioiodine for therapy. This is possibly the earliest use of imaging for theranostics or personalized therapy. For thyroid cancer, imaging

with radioactive iodine is utilized pretherapy to ensure that the tumors accumulate iodine and therefore are appropriate for therapy with iodine-131. In the case illustrated in Fig. 2, imaging shows radioiodine-avid metastases to the brain from thyroid cancer (in addition to metastases to the skeleton and lungs). The MRI, performed before and after therapy with I-131, shows decreased enhancement of a brain metastasis, consistent with response to therapy.

A more recent theranostic system targets prostate specific membrane antigen (PSMA). As the name would suggest, PSMA is overexpressed in prostate cancer but also in tumor vasculature in general (including potentially in brain tumors).

In summary for oncology, improved imaging for both metastatic disease and primary brain tumors is necessary and on the horizon. Future developments through novel tracers and higher resolution scanners may improve grading/staging, differentiating true recurrence from pseudo-progression, and provide evidence to direct treatment planning and if necessary, surgery. In a theranostic paradigm, imaging can stratify patients more likely to benefit from a targeted therapy.

B. Neurodegenerative Diseases

Neurodegenerative diseases represent a broad category of progressive diseases that affect various areas of the nervous system through various pathologic mechanisms. Accumulation of pathologic proteins is thought to be the mechanism or at least a pathognomonic sign for many of these diseases. Take for example two of the most prevalent neurodegenerative diseases, PD, and Alzheimer disease (AD), which are characterized by the accumulation of the proteins alpha-synuclein and amyloid, respectively.

1) Movement Disorders: PD typically presents clinically with tremor, rigidity, and bradykinesia. Clinical molecular imaging of PD utilizes a radioactive dopamine analog, iodine-123 ioflupane, to image the density of presynaptic dopamine transporters in the striatum of the brain. Single photon emission computed tomography (SPECT) images are viewed in the trans-axial plane for dopamine transporter imaging. The anatomy of the striatum resembles a "comma" and thus a normal SPECT scan appears as two "commas." By comparison, PD typically results in greater loss from posterior to anterior so a typical appearance for an abnormal scan demonstrates "periods" (Fig. 3).

While ioflupane SPECT imaging is approved by the USFDA for visual interpretation, software quantification can also be employed as a complementary tool to visual analysis. Computer analysis can generate ratios of various regions of interest in the striatum versus background (occipital region). *Z*-scores are generated showing the deviation of the value from age-matched healthy controls. One of the critical issues is that there is no "magical cut-off" for normal versus abnormal. Utilizing *z*-scores is challenging due to the great variation in the density of dopamine transporter among individuals and also the naturally expected decline with age (Fig. 4). Importantly, software quantification has been demonstrated to add value by allowing nuclear medicine physicians of limited experience to perform similarly to more experienced physicians [item 33) of the Appendix].

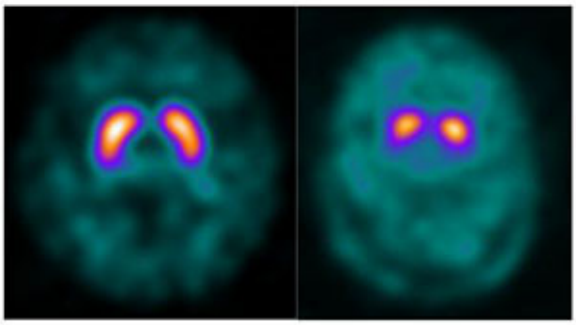

Fig. 3. Normal iodine-123 ioflupane SPECT trans-axial image (left) shows the characteristic comma-shaped striata. In contrast, the scan of a person with PD (right) shows periods due to the typical progressive loss of dopaminergic neurons from posterior to anterior.

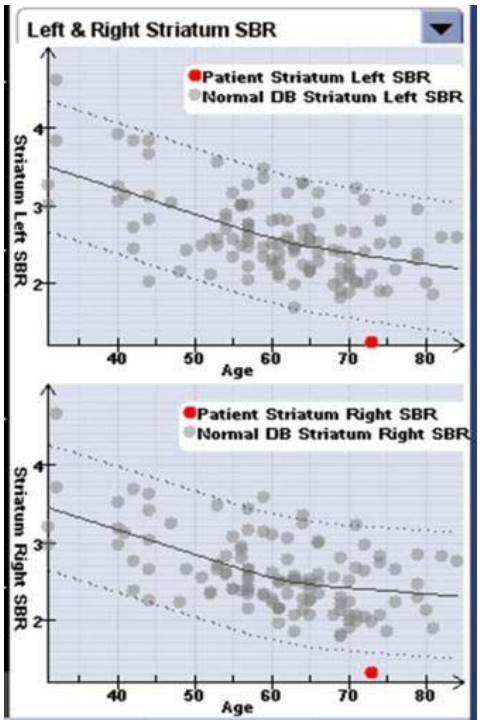

Fig. 4. Graphs from a commercially available software (GE Healthcare) for the quantification of iodine-123 ioflupane SPECT shows the distribution of the striatal binding ratios for the left and right striata for healthy controls over a wide range of ages. The dashed lines indicate two standard deviations. This particular patient with PD (red dot) had severe loss of dopaminergic neurons in both striata that were worse than two standard deviations below age-adjusted normal.

With a dataset of normal and abnormal patients, a receiver operator curve can be developed to optimize a threshold for differentiating between the two groups. This showed that while high sensitivity and specificity can be achieved, normal variability does not allow for perfect separation [item 34) of the Appendix].

While approved by the USFDA to aid in diagnosis, serial dopamine transporter imaging can be used for research to follow progression of disease and also potential response to therapies. SPECT systems with high precision are required to reliably detect small changes or to ensure stability. Further advances in scanner technology which improve

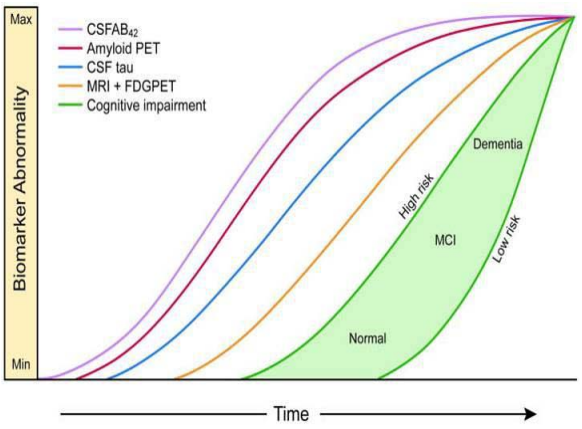

Fig. 5. Model of various biomarkers for AD shows that PET amyloid imaging is the earliest imaging that will be positive/abnormal in persons that are at high risk for developing AD.

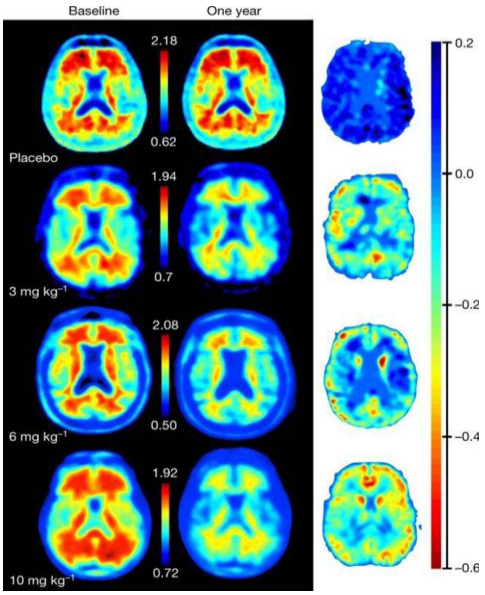

Fig. 6. Examples of PET amyloid imaging from a phase 1 clinical trial with the anti-amyloid antibody aducanumab. From top to bottom, subjects received increasing amount of drug from placebo up to 10 mg/kg. Left column shows baseline PET amyloid imaging. Middle column shows PET amyloid imaging one year after starting drug. Right column displays images subtracting year one from baseline. Subtraction image at the bottom right shows that the greatest decrease in amyloid burden on PET amyloid imaging was observed at the highest dose of the antibody.

resolution may allow better evaluation of subregions of the striatum [item 35) of the Appendix].

Radiomics takes to another level the extraction of information from imaging. One definition of radiomics is "the high throughput extraction of quantitative imaging features or texture from imaging to decode tissue pathology and creating a high-dimensional data set for feature extraction [item 36), 37) of the Appendix]. Radiomic features provide information about the gray-scale patterns, interpixel relationship" [item 36) of the Appendix]. Radiomics, in the form of texture analysis, has been applied to dopamine transporter SPECT imaging and then correlated with clinical assessment [item 38), 39) of the Appendix].

2) Dementia: AD is the most common type of dementia. Due to a combination of multiple factors such as longer life expectancies and the baby boom generation, the prevalence of AD in the United States of America is expected to increase in the coming decades to epidemic proportions. One projection estimates an increase from 5.7 million Americans with AD in 2018 to 14 million by the year 2050. In addition to the suffering of patients, families and friends, AD also inflicts a higher monetary cost. In 2018, an estimated $277 billion in direct costs will be expended caring for patients with AD. With the marked increase in prevalence of AD by 2050, the costs are projected to reach over a staggering $1.1 trillion (www.alz.org).

To aid in the accurate diagnosis of AD, PET amyloid imaging was developed (Fig. 5). There are three USFDA-approved radiopharmaceuticals for PET amyloid imaging of the brain. All three of the approved radiopharmaceuticals demonstrate binding to white matter normally but only bind in the cortical gray matter when amyloid is present. Amyloid is an appropriate target since it is present even early in the disease process; however, it may precede development of symptoms by many years and thus it is possible to be amyloid-positive but not have AD [item 40) of the Appendix].

A major blow to routine use of PET amyloid imaging occurred when Centers for Medicare and Medicaid Services (CMS) decided against reimbursement for the scan because of lack of evidence for clinical utility. The fate of PET amyloid imaging may be best exemplified by three ongoing clinical trials. First, the Imaging Dementia—Evidence for Amyloid Scanning (IDEAS) study seeks to measure the effect of amyloid PET on outcomes in patients (www.ideas-study.org). The trial completed enrollment of over 18 000 patients and collection of outcomes data is in progress. If this paper successfully demonstrates that PET amyloid imaging has a positive impact on patient management and medical outcomes, then CMS reimbursement should follow. Second, a phase 1 clinical trial testing the anti-amyloid antibody aducanumab on patients with prodromal or mild AD utilized PET amyloid imaging as a selection criteria (only amyloid-positive patients by PET were included) [item 41) of the Appendix]. Serial PET amyloid imaging demonstrated a dose-dependent decrease in brain amyloid after one year of therapy with the antibody (Fig. 6). Of critical importance, the antibody also showed a trend toward a dose-dependent slowing of cognitive decline. The antibody is currently being tested in phase 3 clinical trials. Third, the Anti-Amyloid Treatment in Asymptomatic Alzheimer's study (A4 study) is a groundbreaking study utilizing PET amyloid imaging to screen asymptomatic subjects (not patients) for anti-amyloid antibody therapy to prevent the development of AD (www.a4study.org). This trial tests the hypothesis that therapy is more effective if given earlier.

3) Other Considerations: Understanding the Brain: The research applications for brain imaging are diverse and are reported in a separate article in this issue and so here only one illustrative example is given. Application of current brain imaging techniques can contribute to breakthroughs in understanding of the brain's anatomy and physiology.

In 2017, the first report of lymphatic vessels in the human central nervous system was published [item 41) of

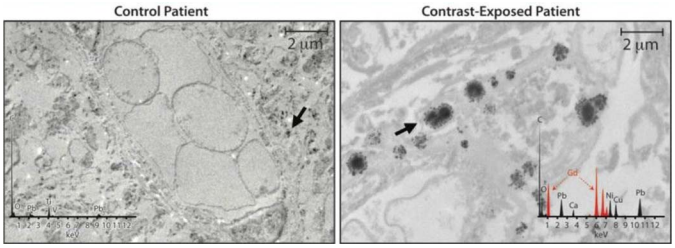

Fig. 7. Right panel is a micrograph from transmission electron microscopy showing gadolinium deposits in brain tissue sample from a patient that received intravenously GBCA. The left panel is a micrograph from a control subject and no gadolinium was found. X-ray spectra for selected foci (arrows) are shown in inset with gadolinium peaks indicated in red.

the Appendix]. Incredibly, such a critical component of anatomy had avoided discovery until so recently. Clinical brain imaging techniques were adapted to reveal vital information on the directionality of flow in meningeal lymphatic vessels [item 42) of the Appendix], adding to the basic understanding of this newly identified feature. In the near future, further adaptations of clinical brain imaging methods to study the lymphatics of the brain may lead to breakthroughs in the understanding of the brain's immune system, neurodegenerative diseases, immunotherapies such as amyloid-targeted antibodies, and metabolism of drugs in the central nervous system.

Safety: Appropriately in the development of any drug or device, safety is paramount, and safety monitoring continues even after approval. In 1997 was the first reported case of a devastating disease that would later be known as nephrogenic systemic fibrosis (NSF) [item 43) of the Appendix]. Almost a decade later, the USFDA released a public health advisory warning about the association of NSF and gadolinium-based contrast agents (GBCAs) used in MRI. NSF is a man-made disease triggered by the intravascular administration of GBCAs in patients with kidney failure [item 44) of the Appendix]. Clinically, the disease is most apparent and typical manifestation is thickening or hardening of the skin which can result in debilitating, decreased mobility of the joints. Systemic involvement can also involve multiple organ systems [item 45) of the Appendix]. Fortunately, through a combination of more judicious use of GBCAs in patients with kidney disease and wider use of more kinetically stable GBCAs, the incidence of NSF rapidly decreased to essentially zero after identification of the connection [item 46) of the Appendix].

But is the story really over? In 2014, Kanda *et al.* [item 47) of the Appendix] reported that increasing signal in certain regions of the brain on T1-weighted imaging correlated with greater numbers of GBCA administrations. Subsequent research has further supported this connection including a study which utilized inductively coupled plasma mass spectrometry to definitively demonstrate gadolinium deposits in the brain from administration of GBCA in patients with normal renal function (Fig. 7) [item 48) of the Appendix].

While no link has been found yet between gadolinium deposition in the brain and neurologic disease, the tragedy of NSF teaches us to be ever vigilant and cautious with the drugs we administer for imaging. In the vast majority of cases, the overall excellent safety record of GBCAs would indicate that the benefit outweighs the risks when deciding whether to administer. However, what if there was an equally efficacious alternative that did not require an exogenous contrast agent? Various MRI techniques have been developed or are in development to reduce our reliance on exogenous contrast agents. One such potential technique is chemical exchange saturation transfer (CEST) [item 49) of the Appendix]. For example, a patient was scanned after radiation therapy for a glioma. CEST MRI demonstrated relative differences in acidosis in brain regions, as evaluated with a multipower method (Fig. 8).

Another alternative is radiomics, which is particularly attractive since it extracts additional information from the image so does not require development of new equipment, sequences, or contrast agents. While outside the realm of discussion here, artificial intelligence will undoubtedly affect clinical imaging in the near future.

In summary, continued vigilance for the safety of the drugs we rely on for optimal imaging is necessity to prevent or mitigate another tragedy like the man-made disease NSF. We should apply the safety lessons we have learned to the development of even safer drugs. Development of novel complementary methods like endogenous contrast methods or radiomics may allow us to avoid the use of exogenous contrast agents particularly in at risk patient populations.

Socioeconomics: PET amyloid imaging teaches an important lesson that approval does not equal reimbursement. Given the high cost of radiopharmaceuticals, utilization will be extremely limited without reimbursement. Keeping this in mind when planning clinical trials may help ensure not only approval but also reimbursement. Also, PET amyloid imaging shows that a radiopharmaceutical can have multiple pathways to reimbursement. If anti-amyloid antibody therapy proves effective, PET imaging may gain approval and reimbursement as part of a theranostic paradigm.

The importance of economics and policy cannot be overstated. Without adequate reimbursement by insurance, imaging will not be accessible to the vast majority of patients. Companies will therefore not have the incentive to develop new pharmaceuticals or imaging equipment. As discussed in the previous section, none of the three USFDA approved PET amyloid imaging agents has been reimbursed by CMS outside of the IDEAS trial. Let us now examine the case of SPECT dopamine transporter imaging of the brain for Parkinsonian syndromes. Currently, the USFDA has approved one radiopharmaceutical, iodine-123 ioflupane, for the evaluation of tremor due to possible Parkinsonian syndrome.

Radiopharmaceuticals generally receive pass-through status for the first 2-3 years after USFDA approval which assures that CMS payment is adequate to ensure that imaging centers will not lose money on the new drug. Now that the pass-through period has expired, current reimbursement by CMS for hospital-based iodine-123 ioflupane imaging is less than the cost of the radiopharmaceutical (i.e., hospitals lose money when they perform iodine-123 ioflupane SPECT). The profit–loss margin changes depending on an imaging practice's payor mix and designation as outpatient versus hospital-based scanners [item 50) of the Appendix].

Reimbursement always has been but is now an increasingly more difficult hurdle for imaging. Reimbursement

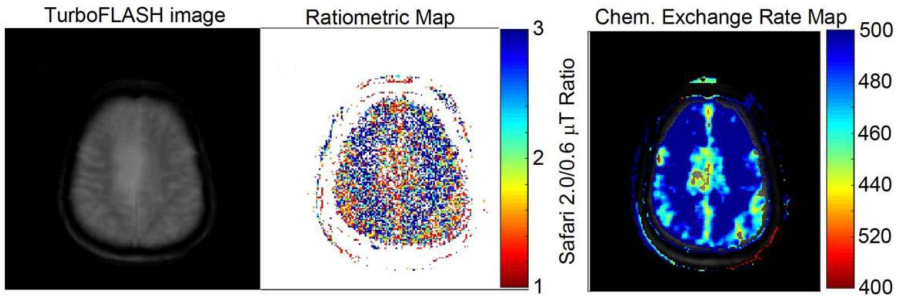

Fig. 8. CEST MRI may differentiate tumor recurrence from radiation-induced inflammation. (a) Standard TurboFLASH MR image shows a large region of inflammation in a patient with glioblastoma treated with radiation therapy. Tumor recurrence cannot be identified within this region of inflammation. (b) Patient was also analyzed with SAFARI MRI, a variation of CEST MRI performed at 2 and 6 uT saturation powers. (c) Chemical exchange rate map derived from multipower SAFARI MRI showed regions with low chemical exchange rates between endogenous proteins and water. Because chemical exchange between proteins and water is base catalyzed, the low chemical exchange rate was attributed to low pH, which was likely caused by acidosis from dysregulated metabolism in a recurring solid tumor (Image courtesy of Mark Pagel).

challenges start at the very beginning with, for example, PET amyloid imaging but also continue in later years as with dopamine transporter SPECT. For proper payment of imaging, we have the onus of proving both efficacy and value. Value-based healthcare research has reached all areas of medicine including imaging. Therefore, planning and conducting value-based research for a drug or radiopharmaceutical should be a continuous process. One novel approach for dopamine transporter SPECT asked the consumer, the patient, directly [item 51) of the Appendix]. In a survey, the majority of patients felt that the dopamine transporter imaging improved the level of confidence in their diagnosis. In the same survey, a majority of patients would recommend, probably or definitely, the use of imaging for other patients like themselves.

In my opinion, we need value-based research at all levels: institutional, regional, national, and international. Physicians and scientists need to collaborate with insurers, companies, and societies to prove the value of our tests to the patients we serve. Finally, involving and recruiting patients to be advocates will lend their voices to ours when making our case to insurers.

Summary: In summary, the wide diversity of disorders involving the brain demand that research be commensurately innovative. We are on the cusp of many breakthroughs in diagnosis, treatment and their combination in the form of theranostics. But, the work is never done since we must always remain vigilant for unforeseen issues of patient safety. Many challenges, both scientific and socioeconomic, will only be overcome through teamwork across many disciplines to ensure that patients benefit from research.

RICHARD E. CARSON
(A Perspective on Requirements for Clinical Research)
Department of Radiology and Biomedical Imaging
School of Medicine
Yale University
New Haven, CT 06520 USA
e-mail: richard.carson@yale.edu
PHILLIP H. KUO
(Clinical Needs in Brain Imaging: A Physician-Scientist's Point of View)
Department of Medical Imaging
University of Arizona, Banner University Medical Center
Tucson, AZ 85724 USA
Department of Biomedical Engineering
University of Arizona, Banner University Medical Center
Tucson, AZ 85724 USA

APPENDIX
RELATED WORK

1) H. W. de Jong *et al.*, "Performance evaluation of the ECAT HRRT: An LSO-LYSO double layer high resolution, high sensitivity scanner," *Phys. Med. Biol.*, vol. 52, no. 5, pp. 1505–1526, 2007.
2) A. J. González, F. Sánchez, and J. M. Benlloch, "Organ dedicated molecular imaging systems" *IEEE Trans. Radiat. Plasma Med. Sci.*, vol. 2, no. 5, pp. 388–403, Sep. 2018.
3) R. E. Carson *et al.*, "Comparison of bolus and infusion methods for receptor quantitation: Application to [18F]cyclofoxy and positron emission tomography," *J. Cereb. Blood Flow Metab.*, vol. 13, no. 1, pp. 24–42, 1993.
4) R. B. Innis *et al.*, "Consensus nomenclature for *in vivo* imaging of reversibly binding radioligands," *J. Cereb. Blood Flow Metab.*, vol. 27, no. 9, pp. 1533–1539, 2007.
5) C. S. Li *et al.*, "Decreased norepinephrine transporter availability in obesity: Positron emission tomography imaging with (S,S)-[11C]O-methylreboxetine," *NeuroImage*, vol. 86, pp. 306–310, Feb. 2014.
6) M. Naganawa *et al.*, "Tracer kinetic modeling of [11C]AFM, a new PET imaging agent for the serotonin transporter," *J. Cereb. Blood Flow Metab.*, vol. 33, no. 12, pp. 1886–1896, 2013.
7) D. Matuskey *et al.*, "Dopamine D_3 receptor alterations in cocaine-dependent humans imaged with [C](+)PHNO," *Drug Alcohol Dependence*, vol. 139, pp. 100–105, Jun. 2014.
8) M. Naganawa *et al.*, "Evaluation of the agonist PET radioligand [^{11}C]GR103545 to image kappa opioid receptor in humans: Kinetic model selection, test-retest reproducibility and receptor occupancy by the antagonist PF-04455242," *NeuroImage*, vol. 99, pp. 69–79, Oct. 2014.
9) A. D. Joshi, J. A. Fessler, and R. A. Koeppe, "Improving PET receptor binding estimates from Logan plots using principal component analysis," *J. Cereb. Blood Flow Metab.*, vol. 28, no. 4, pp. 852–865, 2008.
10) F. E. Turkheimer, M. Brett, D. Visvikis, and V. J. Cunningham, "Multiresolution analysis of emission tomography images in the wavelet domain," *J. Cereb. Blood Flow Metab.*, vol. 19, no. 11, pp. 1189–1208, 1999.
11) B. T. Christian, N. T. Vandehey, J. M. Floberg, and C. A. Mistretta, "Dynamic PET denoising with HYPR processing," *J. Nucl. Med.*, vol. 51, no. 7, pp. 1147–1154, 2010.
12) M. Germino, J. D. Gallezot, J. Yan, and R. E. Carson, "Direct reconstruction of parametric images for brain PET with event-by-event motion correction: Evaluation in two tracers across count levels," *Phys. Med. Biol.*, vol. 62, no. 13, pp. 5344–5364, 2017.
13) J.-D. Gallezot, Y. Lu, M. Naganawa, and R. E. Carson, "Parametric imaging with PET and SPECT," *IEEE Trans. Radiat. Plasma Med. Sci.*, to be published. doi: 10.1109/TRPMS.2019.2908633.
14) S. J. Finnema *et al.*, "Imaging synaptic density in the living human brain," *Sci. Transl. Med.* vol. 8, no. 348, 2016, Art. no. 348ra96.

15) S. J. Finnema *et al.*, "Kinetic evaluation and test-retest reproducibility of [11C]UCB-J, a novel radioligand for positron emission tomography imaging of synaptic vesicle glycoprotein 2A in humans," *J. Cereb. Blood Flow Metab.*, vol. 38, no. 11, pp. 2041–2052, 2018.
16) P. D. Worhunsky *et al.*, "Regional and source-based patterns of [^{11}C]-(+)-PHNO binding potential reveal concurrent alterations in dopamine D_2 and D_3 receptor availability in cocaine-use disorder," *NeuroImage*, vol. 148, pp. 343–351, Mar. 2017.
17) V. L. Villemagne, V. Dore, S. C. Burnham, C. L. Masters, and C. C. Rowe, "Imaging tau and amyloid-βproteinopathies in Alzheimer disease and other conditions," *Nat. Rev. Neurol.*, vol. 14, no. 4, pp. 225–236, 2018.
18) T. G. Lohith *et al.*, "Brain imaging of Alzheimer dementia patients and elderly controls with ^{18}F-MK-6240, a PET tracer targeting neurofibrillary tangles," *J. Nucl. Med.*, vol. 60. pp. 107–114, Jan. 2019.
19) M. Lehmann *et al.*, "Diverging patterns of amyloid deposition and hypometabolism in clinical variants of probable Alzheimer's disease," *Brain J. Neurol.*, vol. 136, no. 3, pp. 844–858, 2013.
20) M. K. Chen *et al.*, "Assessing synaptic density in Alzheimer disease with synaptic vesicle glycoprotein 2A positron emission tomographic imaging," *JAMA Neurol.*, vol. 75, no. 10, pp. 1215–1224, 2018.
21) K. Erlandsson, I. Buvat, P. H. Pretorius, B. A. Thomas, and B. F. Hutton, "A review of partial volume correction techniques for emission tomography and their applications in neurology, cardiology and oncology," *Phys. Med. Biol.*, vol. 57, no. 2, pp. 119–159, 2012.
22) P. Zanotti-Fregonara, K. Chen, J. S. Liow, M. Fujita, and R. B. Innis, "Image-derived input function for brain PET studies: Many challenges and few opportunities," *J. Cereb. Blood Flow Metab.*, vol. 31, no. 10, pp. 1986–1998, 2011.
23) E. K. Fung and R. E. Carson, "Cerebral blood flow with [15O]water PET studies using an image-derived input function and MR-defined carotid centerlines," *Phys. Med. Biol.*, vol. 58, no. 6, pp. 1903–1923, 2013.
24) R. E. Carson, W. C. Barker, J.-S. Liow, and C. A. Johnson, "Design of a motion-compensation OSEM list-mode algorithm for resolution-recovery reconstruction of the HRRT," in *Proc. IEEE Nucl. Sci. Symp. Med. Imag. Conf.*, Portland, OR, USA, 2003, pp. 3281–3285.
25) X. Jin, T. Mulnix, J. D. Gallezot, and R. E. Carson, "Evaluation of motion correction methods in human brain PET imaging—A simulation study based on human motion data," *Med. Phys.*, vol. 40, no. 10, 2013, Art. no. 102503.
26) P. J. Schleyer *et al.*, "Detecting and estimating head motion in brain PET acquisitions using raw time-of-flight PET data," *Phys. Med. Biol.*, vol. 60, no. 6, pp. 6441–6458, 2015.
27) O. V. Olesen *et al.*, "List-mode PET motion correction using markerless head tracking: Proof-of-concept with scans of human subject," *IEEE Trans. Med. Imag.*, vol. 32, no. 2, pp. 200–209, Feb. 2013.
28) P. Lecoq, "Pushing the limits in time-of-flight PET imaging," *IEEE Trans. Radiat. Plasma Med. Sci.*, vol. 1, no. 6, pp. 473–485, Nov. 2017.
29) Y. Yang, M. Z. He, T. Li, and X. Yang, "MRI combined with PET-CT of different tracers to improve the accuracy of glioma diagnosis: A systematic review and meta-analysis," *Neurosurg. Rev.*, vol. 6, p. 149, Sep. 2017. [Online]. Available: http://doi.org/10.1007/s10143-017-0906-0
30) S. Kebir *et al.*, "Late pseudoprogression in glioblastoma: Diagnostic value of dynamic O-(2-[18F]fluoroethyl)-L-tyrosine PET," *Clin. Cancer Res.*, vol. 22, no. 9, pp. 2190–2196, 2016. [Online]. Available: http://doi.org/10.1158/1078-0432.CCR-15-1334
31) A. Karlberg *et al.*, "Multimodal ^{18}F-Fluciclovine PET/MRI and ultrasound-guided neurosurgery of an anaplastic oligodendroglioma," *World Neurosurg.*, vol. 108, Dec. 2017, Art. no. e1-989. [Online]. Available: http://doi.org/10.1016/j.wneu.2017.08.085
32) D. Y. Lee and K. C. Li, "Molecular theranostics: A primer for the imaging professional," *Amer. J. Roentgenol.*, vol. 197, no. 2, pp. 318–324, 2011. [Online]. Available: http://doi.org/10.2214/AJR.11.6797
33) J. Booij *et al.*, "Diagnostic performance of the visual reading of ^{123}I-ioflupane SPECT images when assessed with or without quantification in patients with movement disorders or dementia," *J. Nucl. Med.*, vol. 58, no. 11, pp. 1821–1826, 2017. [Online]. Available: http://doi.org/10.2967/jnumed.116.189266
34) P. H. Kuo *et al.*, "Receiver-operator-characteristic analysis of an automated program for analyzing striatal uptake of ^{123}I-Ioflupane SPECT images: Calibration using visual reads," *J. Nucl. Med. Technol.*, vol. 41, no. 1, pp. 26–31, 2013.
35) I. G. Zubal *et al.*, "Optimized, automated striatal uptake analysis applied to SPECT brain scans of Parkinson's disease patients," *J. Nucl. Med.*, vol. 48, no. 6, pp. 857–864, 2007.
36) V. Parekh and M. A. Jacobs, "Radiomics: A new application from established techniques," *Exp. Rev. Precision Med. Drug Develop.*, vol. 1, no. 2, pp. 207–226, 2016. [Online]. Available: http://doi.org/10.1080/23808993.2016.1164013
37) M. Hatt, C. Parmar, J. Qi, and I. El Naqa, "Machine (deep) learning methods for image processing and radiomics," *IEEE Trans. Radiat. Plasma Med. Sci.*, vol. 3, no. 2, pp. 104–108, Mar. 2019.
38) A. Rahmim *et al.*, "Application of texture analysis to DAT SPECT imaging: Relationship to clinical assessments," *NeuroImage Clin.*, vol. 12, pp. e1–e9, Feb. 2016. doi: 10.1016/j.nicl.2016.02.012.
39) R. Mabrouk, B. Chikhaoui, and L. Bentabet, "Machine learning based classification using clinical and DaTSCAN SPECT imaging features: A study on Parkinson's disease and SWEDD," *IEEE Trans. Radiat. Plasma Med. Sci.*, vol. 3, no. 2, pp. 170–177, Mar. 2019.
40) J. Sevigny *et al.*, "Addendum: The antibody aducanumab reduces Aβ plaques in Alzheimer's disease," *Nature*, vol. 546, no. 7659, p. 564, 2017. doi: 10.1038/nature22089.
41) M. Absinta *et al.*, "Human and nonhuman primate meninges harbor lymphatic vessels that can be visualized noninvasively by MRI," *eLife*, vol. 6, Oct. 2017, Art. no. e29738. [Online]. Available: http://doi.org/10.7554/eLife.29738
42) P. H. Kuo, C. Stuehm, S. Squire, and K. Johnson, "Meningeal lymphatic vessel flow runs countercurrent to venous flow in the superior sagittal sinus of the human brain," *Tomography*, vol. 4, no. 3, pp. 99–104, 2018. doi: 10.18383/j.tom.2018.00013.
43) S. E. Cowper *et al.*, "Scleromyxoedema-like cutaneous diseases in renal-dialysis patients," *Lancet*, vol. 356, no. 9234, pp. 1000–1001, 2000.
44) P. H. Kuo, E. Kanal, A. K. Abu-Alfa, and S. E. Cowper, "Gadolinium-based MR contrast agents and nephrogenic systemic fibrosis," *Radiology*, vol. 242, no. 3, pp. 647–649, 2007. doi: 10.1148/radiol.2423061640.
45) J. C. Weinreb and P. H. Kuo, "Nephrogenic systemic fibrosis," *Magn. Reson. Imag. Clinics North America*, vol. 17, no. 1, pp. 159–167, 2009. doi: 10.1016/j.mric.2009.01.003.
46) P. H. Kuo, "Gadolinium-containing MRI contrast agents: Important variations on a theme for NSF," *J. Amer. College Radiol.*, vol. 5, no. 1, pp. 29–35, 2008. doi: 10.1016/j.jacr.2007.08.014.
47) T. Kanda, K. Ishii, H. Kawaguchi, K. Kitajima, and D. Takenaka, "High signal intensity in the dentate nucleus and globus pallidus on unenhanced T1-weighted MR images: Relationship with increasing cumulative dose of a gadolinium-based contrast material," *Radiology*, vol. 270, no. 3, pp. 834–841, 2014. doi: 10.1148/radiol.13131669.
48) R. J. McDonald *et al.*, "Gadolinium deposition in human brain tissues after contrast-enhanced MR imaging in adult patients without intracranial abnormalities," *Radiology*, vol. 285, no. 2, pp. 546–554, 2017. doi: 10.1148/radiol.2017161595.
49) K. M. Jones *et al.*, "Clinical translation of tumour acidosis measurements with acidoCEST MRI," *Mol. Imag. Biol.*, vol. 19, no. 4, pp. 617–625, 2017.
50) M. F. Covington, N. A. McMillan, and P. H. Kuo, "Impact of reimbursement cuts on the sustainability and accessibility of dopamine transporter imaging," *J. Amer. College Radiol.*, vol. 13, no. 9, pp. 1039–1043, 2016.
51) M. Covington *et al.*, "Patient survey on satisfaction and impact of ^{123}I-ioflupane dopamine transporter imaging," *PLoS ONE*, vol. 10, no. 7, 2015, Art. no. e0134457. doi: 10.1371/journal.pone.0134457.